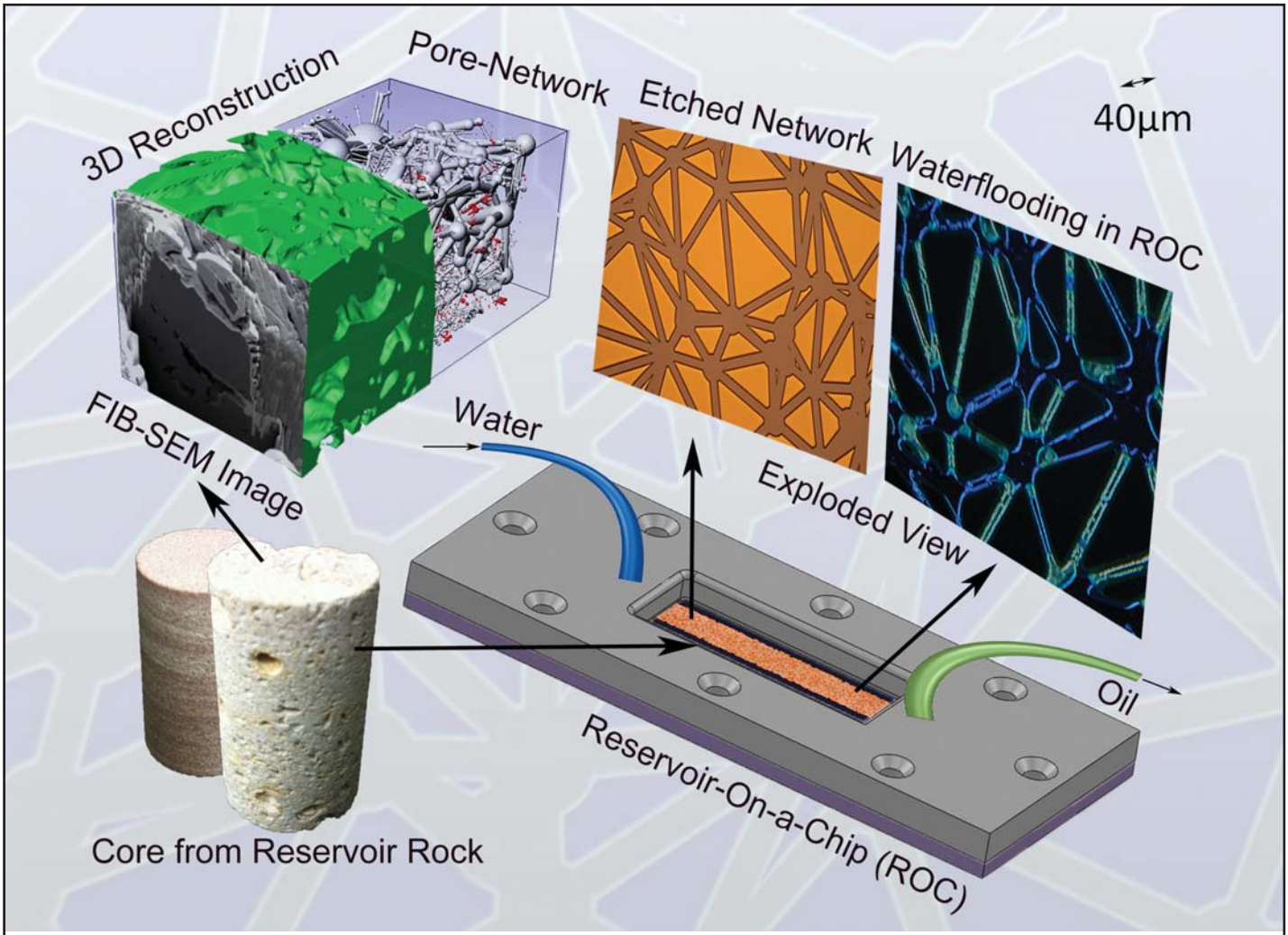

Featuring research from the Micro and Nano-Scale Transport Laboratory, Department of Mechanical Engineering, University of Alberta.

Title: Reservoir-on-a-Chip (ROC): A new paradigm in reservoir engineering

ROC (Reservoir-on-a-Chip) is a novel miniaturization approach to study oil recovery in a microfluidic device, which enables researchers to understand the pore-scale transport relevant to reservoir engineering.

As featured in:

See Aksimentiev *et al.*, *Lab Chip*, 2011, **11**, 3766.

RSC Publishing

www.rsc.org/loc

Registered Charity Number 207890

Lab on a Chip

Dynamic Article Links

Cite this: *Lab Chip*, 2011, **11**, 3785

www.rsc.org/loc

PAPER

Reservoir-on-a-Chip (ROC): A new paradigm in reservoir engineering†

Naga Siva Kumar Gunda,[a] Bijoyendra Bera,[a] Nikolaos K. Karadimitriou,[b] Sushanta K. Mitra*[a] and S. Majid Hassanizadeh[b]

Received 27th June 2011, Accepted 13th September 2011
DOI: 10.1039/c1lc20556k

In this study, we design a microfluidic chip, which represents the pore structure of a naturally occurring oil-bearing reservoir rock. The pore-network has been etched in a silicon substrate and bonded with a glass covering layer to make a complete microfluidic chip, which is termed as 'Reservoir-on-a-chip' (ROC). Here we report, for the first time, the ability to perform traditional waterflooding experiments in a ROC. Oil is kept as the resident phase in the ROC, and waterflooding is performed to displace the oil phase from the network. The flow visualization provides specific information about the presence of the trapped oil phase and the movement of the oil/water interface/meniscus in the network. The recovery curve is extracted based on the measured volume of oil at the outlet of the ROC. We also provide the first indication that this oil-recovery trend realized at chip-level can be correlated to the flooding experiments related to actual reservoir cores. Hence, we have successfully demonstrated that the conceptualized 'Reservoir-on-a-Chip' has the features of a realistic pore-network and in principle is able to perform the necessary flooding experiments that are routinely done in reservoir engineering.

1. Introduction

A typical oil field (or reservoir) extends a few hundred meters below the earth's surface and is porous in nature, containing oil and water phases in an interconnected three-dimensional (3D) network of pores. When extracting oil by normal pressurization is no longer possible from these reservoirs, secondary and tertiary extraction methods involving injection of a second phase are generally followed. Waterflooding is one such principal method (secondary extraction), where water is the injected fluid phase in order to displace the resident oil phase in the reservoir rock.[1] Traditional lab-scale flooding experiments use a core from a sample reservoir-rock for experimentation and collection of recovery data,[2] known as core-flooding experiments. However, the fluid transport processes in a reservoir occur at a pore-scale, the smallest structural feature in such reservoirs (in order of nanometre to millimetre). In order to develop efficient recovery methods, one needs to understand the underlying physical processes that occur at the pore-scale.

A large body of literature exists regarding the investigation of multi-phase fluid flow in pore-scale. The extensively employed technique in such investigations is pore network modeling (network simulators).[3–5] Pore network models need a complete description of geometrical and topological information of pore space and a complete understanding of physical processes occurring at pore-scale.[3,4] The geometrical and topological information of pore space of rock is represented with a network of pores (large void spaces) connected to throats (small constrictions).[3,4,6] This type of representation of porous media with a network of pores was first developed by Fatt in the 1950's.[7] Heiba *et al.*[8] used percolation theory to explain the multi-phase transport properties. Lenormand *et al.*[9,10] studied the pore scale displacement mechanisms for both drainage and imbibition directly using etched ordered networks in glass. These etched networks are known as micromodels. The results obtained in experiments are correlated and included in the pore-network models to compute multiphase transport properties.[3] However, these estimated properties are limited to a simplified network of pores and do not represent the actual pore space.[4] With the improvement of high-resolution digital imaging and computerized image analysis, researchers have been able to quantify rock microstructure.[5,6,11,12] It is now possible to reconstruct the 3D pore space using micro-computed tomography (micro-CT),[5,6,11–14] focused ion beam-scanning electron microscope (FIB-SEM),[13] nuclear magnetic resonance (NMR) imaging[15,16] or ultrasonic scanning.[17] Multiphase flow properties are calculated with direct numerical simulations on 3D reconstructed pore space using the finite element method (FEM),[18,19] finite volume method (FVM),[20,21] finite difference method (FDM)[22] or lattice Boltzmann method (LBM).[23–27] However, these types of simulations are computationally expensive, limited to small sample sizes and not possible to scale-up to actual field scale.[3,4] Hence,

[a]*Department of Mechanical Engineering, Micro and Nano-Scale Transport Laboratory, University of Alberta, Edmonton, Canada T6G 2G8. E-mail: sushanta.mitra@ualberta.ca; Fax: +1-780-492-2200; Tel: +1-780-492-5017*

[b]*Department of Earth Sciences, Universiteit Utrecht, Budapestlaan, Utrecht, 3584CD, The Netherlands*

† Electronic supplementary information (ESI) available. See DOI: 10.1039/c1lc20556k

physically realistic pore-network structures representing the actual pore space is extracted to simplify the simulations and improve the conventional pore network models.[12,28,29] This physically realistic representation provides a direct mapping of pore bodies and throats. Various multiphase transport properties are computed using these physically realistic network models. It is possible to scale up the sample sizes using stochastic random network generators to estimate the multiphase properties.[30,31] However, in numerical modeling, the properties are predicted with arbitrary wetting characteristics.[3–5] Experimental investigations at pore-scale are required to validate or improve the numerical studies. Direct visualization of the multiphase transport process is difficult because of the non-transparent nature of the porous media.[32]

Oren and Pinczewski[33] have performed three-phase flow experiments in oil-wet micromodels and Van Dijke *et al.*[34,35] have extended such experiments for water-alternating gas injection in oil-wet glass micromodels. Sohrabi *et al.*[36] have also studied water alternating gas injection using high pressure micromodels in both oil-wet and mixed-wet systems. Polymer flooding in glass micromodels[37,38] has been studied as well, and Meybodi *et al.*,[39] Jamaloei and Kharrat[40–42] have performed detailed investigations of displacement behaviors in this context. Perrin *et al.*[43] have even investigated the quantitative information of the velocity field inside such pore network micromodels using micro-PIV (particle image velocimetry). The studies mentioned here do not use actual realistic pore spaces of rock samples and are limited to two-dimensional (2D) representations. However, Bowden *et al.*[44,45] and others[33,34] have represented the porous medium in the form of packed beds to study the multiphase flows. They even demonstrated flooding experiments to determine recovery efficiency in such packed beads.[44] Recently, Sen *et al.*[46] computed the velocity components in a packed bed mimicking porous media using micro-PIV. These experiments are limited to engineered porous media which often include random or orderly packed granular systems without having a realistic representation of pore connectivity. In a more recent effort, Berejnov *et al.*[47] has represented the porous medium as a structured microfluidic network with prescribed geometries. In their experiments, they have performed investigations of fluid flow parameters and wettability in such networks, by tuning surface properties. Aktas *et al.*[48] and Buchgraber *et al.*[49,50] have conducted displacement experiments in etched glass micromodels represented by a repeated pattern of a SEM image of sandstone. A single SEM image of sandstone still lacks the connectivity of actual pore space.

In this study, we demonstrate a novel method for the design and fabrication of a porous medium, where a pore network representation of the porous medium has been replicated in a microfluidic chip. Conceptually, the entire porous reservoir pertaining to oil/gas recovery has been miniaturized, without losing the pore-scale characteristic of its complex features. To the best of the authors' knowledge, for the first time waterflooding experiments are attempted on such a microfluidic chip to obtain the desired oil recovery curves. Hence, we coin a new term 'Reservoir-on-a-Chip' (ROC) to refer to this unique microfluidic chip, which is believed to be the first of its kind. It is to be kept in mind that the word "reservoir" traditionally refers to the inlet and outlet fluid storage spaces in a typical LOC. Here the intent is to extend the traditional concept of LOC to reservoir engineering and hence the term "reservoir" refers to the natural occurring porous media (geological formation) in which oil/water/gas phases co-exist.

2. Reservoir-on-a-Chip: ROC

Here, we describe the conceptual map for fabricating a Reservoir-on-a-Chip. The advent of modern imaging techniques has made it possible to describe the pore architecture of the porous medium directly.[51–54] Bera *et al.*[13] have demonstrated the characterization of reservoir-rock cores using methods such as micro-computed tomography (micro-CT) and focused ion beam-scanning electron microscopy (FIB-SEM). They quantified the pore space in terms of porosity, pore connectivity between pores of various shape and size, as well as pore-volume distribution.

These well-defined methods are followed for investigating the pore space in a sandstone/carbonate dolomitic core,[13] some of the principal oil-bearing rock specimens. FIB-SEM can be used to characterize the internal micro-structure, and then the obtained pore-structure data can be reconstructed by using an image analysis software (for *e.g.*, Avizo, Temography, Fiji, Simpleware Scan IP *etc.*). The obtained 3D reconstructed pore-space is a result of extensive image-processing steps, which capture the most realistic representation of a reservoir. Using maximal ball algorithm,[28,29] medial axis algorithm[12] or triangulation,[55] this pore-space is converted to a network containing pores and throats. Proper care has been taken to extract the information without losing any microstructural details. Such network representation of the porous reservoir is more realistic than adhoc attribution of pores and throats to a pore network model or representing the porous medium as packed bed of spheres or sand grains.[33,34] The microstructural information is extracted from the 3D reconstructed images by direct mapping of pores and throats. The extracted microstructural information is used to represent the 2D pore-network using stochastic random network generators[30,31] or Delaunay triangulation.[56] In this way, percolation of phases was ensured. This stochastic method can also be used to produce bigger sample sizes with realistic pore space information. Then taking this network image, one can etch the features in silicon or glass using photolithography processes. Appropriate microfluidic connections can be made on the microfabricated chip for subsequent experiments related to water flooding.

Thus, keeping intact the essence of a real reservoir-rock, the pore-network is fabricated on a silicon substrate based on the state-of-art microfabrication techniques. A covering glass layer with inlet-outlet ports is bonded with the network layer, making it a complete microfluidic device. We call this novel chip 'Reservoir-on-a-chip' (ROC). Fig. 1 illustrates the conceptual mechanisms of converting a reservoir-rock specimen to an ROC, which facilitates the investigation of the pore-scale transport pertaining to oil recovery processes in reservoir engineering.

3. Experimental section

3.1. Pore network design

A key step in the microfabrication process is to fabricate a mask which has the appropriate features replicating a porous medium.

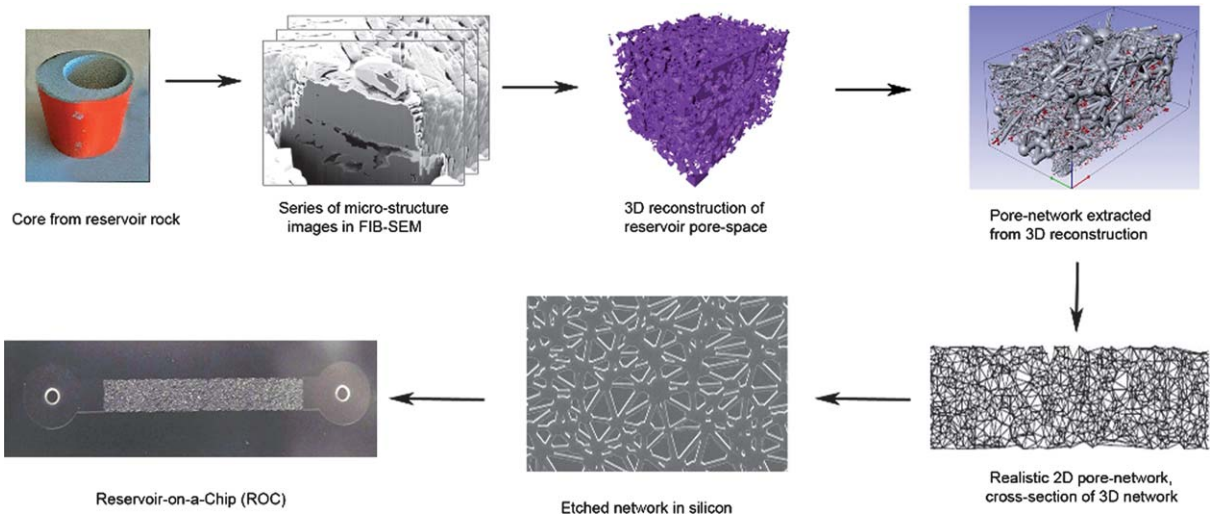

Fig. 1 The conceptual flow-map for 'Reservoir-on-a-Chip'.

To this effort, a 2D pore-throat network has to be designed based on the realistic reconstructed pore space of reservoir-cores, as explained in the previous section. Details of the network design are described by Karadimitriou *et al.*[56] It is observed that Delaunay triangulation is a suitable way to represent a typical porous medium in terms of the number of pores, throats and their connectivity.[55] In the present study, the 2D network was designed with 2000 pores and 6000 throats using Delaunay triangulation. In this type of triangulation, the length of a throat is defined as the difference between the distance separating the pore-centres and the summation of the individual pore radius. The width of a throat is assigned such that it is always less than (not more than 90%) the smallest pore it is connected to. The mean pore size of the network is 40 μm and a log-normal distribution is adopted for pores and throats. The smallest pore in the present network is 25 μm.

A Delaunay triangulation routine in Matlab (Mathworks Inc., Natwick, MA, USA) is used for generating the network. Based on the triangulation steps, the co-ordinates of the pore centres are chosen, and the network is created. The output from the Matlab routine, in the form of a pore–throat network, was then imported into AutoCAD (Version 2010, Autodesk Inc., San Rafael, CA), using LISP (list processing language). Furthermore, the AutoCAD file containing the imprint of the network is modified to accommodate the inlet and outlet ports and suitable entrance and exit regions located at either side of the original pore network.

As shown in Fig. 2(a), the final design of the pore network, which is transferred to a glass substrate (acting as a mask in the microfabrication step), consists of the pore–throat structure (35 mm in length and 5 mm in width), rectangular entrance and exit regions (5 mm length and 5 mm width) and circular inlet-outlet regions (10 mm diameter). Fig. 2(b) illustrates the nature of the distribution of pores and throats in the network.

3.2. Fabrication and characterization of ROC

In this section, we provide some key steps involved in fabricating the ROC on a silicon substrate. The microfluidic chip is fabricated on a 4″ diameter circular silicon substrate (0.5 mm thick, Silicon Valley Microelectronics Inc., Santa Clara, CA). After cleaning the substrates in a standard piranha solution (H_2SO_4 and H_2O_2 in 3 : 1 ratio; 30 min) and drying, a standard photolithography technique is used for transferring the designed pore network from the patterned mask to the substrate. We used a positive photomask on a glass wafer (125 mm × 125 mm square plate and 2 mm thick) with a chrome coating. The detailed patterned structure of the mask is shown in Fig. 2(a). A 2.5 μm thick layer of UV sensitive photo-resist HPR 506 (Fujifilm Electronic Materials Inc., Mesa, Arizona) on the silicon substrate is used during this process. Inductively coupled plasma reactive ion etching (ICPRIE) is used for dry-etching the substrate with the desired pattern on silicon (STS, Newport, UK). An etch-rate of 4.95 μm min^{-1} is selected in this step. The covering layer with inlet-outlet ports is fabricated on glass (Borofloat, 100 mm × 100 mm square, 1 mm thick). Abrasive water-jetting (2652 JetMachining Center, OMAX, Kent, WA) is used for drilling these holes on a covering glass layer, and bonded with the silicon layer using SUSS bonder (CB6L, SUSS Microtec, Garching).

The average depth, roughness and pore–throat sizes of the fabricated ROC is measured using scanning electron microscopy (ZEISS, Germany) along with a surface profilometer (Ambios XP 300, Ambios Technology Inc, Santa Cruz, CA). The average depth of the etched silicon network is 40.93 μm. The roughness of the ROC is in the order of 4–6 nm, which is negligible compared to the depth of the fabricated channel. SEM characterization shows that almost vertical wall-profile (Fig. 2(c)) in the ROC has been achieved, which ensures the proper replication of the pore network in the fabricated ROC. Fig. 2(e) shows the complete ROC (containing 2000 pores and 6000 throats), in which subsequent experiments are performed. The fabricated ROC is water-wet due to the following reasons: (1) Piranha cleaning of silicon and glass layers before bonding, results in the formation of a very thin layer of oxide film on the surface of the silicon. This can contribute to a minor modification of the silicon surface wettability towards water wet.[57] (2) During anodic bonding of silicon to glass, silicon is oxidized at 315 °C, which forms a solid

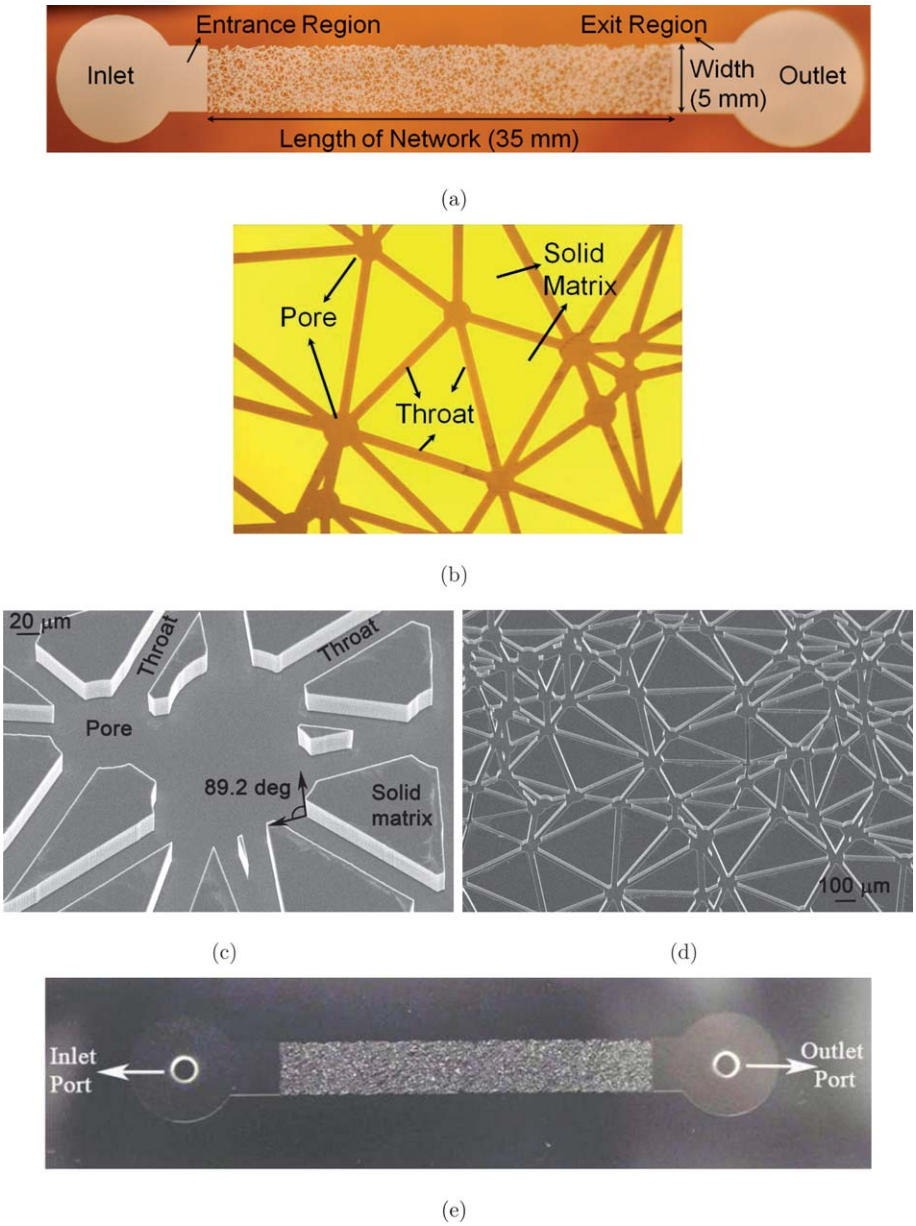

Fig. 2 Reservoir-on-a-Chip (ROC) (a) pore network patterned on glass mask, along with inlet-outlet and entrance-exit regions; (b) the pore and throat distribution of the network in the mask; (c) near-vertical wall-profile obtained in the network, fabricated on silicon; (d) pore–throat distribution of network in etched silicon; (e) complete ROC obtained in etched silicon after covering with glass layer.

film of silicon dioxide. This caused the ROC to exhibit a permanent water-wet behavior.[48]

3.3. Waterflooding experiments

A complete realization of the 'Reservoir-on-a-Chip' can be achieved once the fabricated ROC is used to perform recovery experiments, analogous to those done in traditional core-flooding and reported micromodel experiments. In this section, we describe the waterflooding experiments with a ROC, and discuss the subsequent recovery data.

The experimental set-up for waterflooding with ROC (Fig. 3) includes a microscope (180× magnification, 1.3 Mpixel CMOS image sensor, ViewSolutions GE-5, Howard Electronic Instruments Inc., El Dorado, KS) for the visualization of oil/water phases in the 'Reservoir-on-a-Chip'. The ROC is placed inside a custom-made casing, with microfluidic connectors attached, for controlling fluid flow and efficient visualization. We illuminated the ROC using a light source from the top to capture high-resolution videos and images of fluid transport within the network. M1 lubricant oil (L.S. Starrett Company, Athol, MA; specific gravity ~788 at 15.5 °C, viscosity ~2.2 cSt) has been used as the oil phase to be displaced by water. This lubricant oil is representative of light oils, which can be obtained from crude oils after refining. Hadia *et al.*[2] used paraffin oils (light and heavy) for their study of core flooding experiments. The oil used in the present work has similar properties to that of the light paraffin oils used by Hadia *et al.*[2] This clean M1 lubricant oil is employed

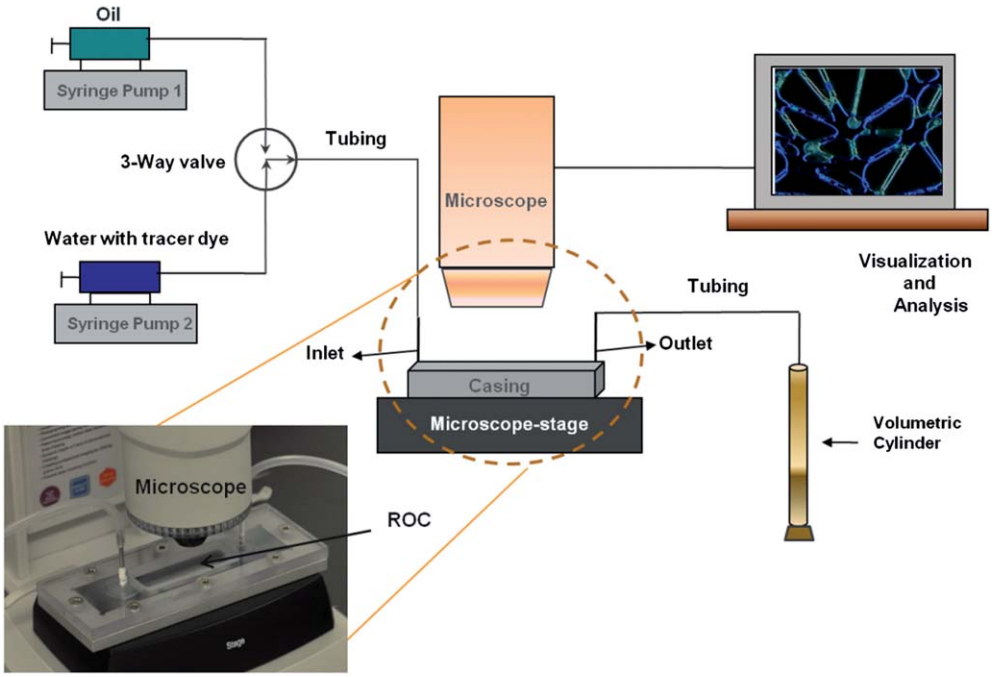

Fig. 3 Schematic of the experimental set-up used in performing waterflooding experiments with ROC; inset illustrates the magnified image of ROC housed in a casing, placed under the microscope for flow visualization experiments.

in the present work to demonstrate waterflooding. For properly distinguishing the oil/water interface during the fluid transport, a blue tracer dye (Bright Dyes, Promag Enviro systems Inc., Burnaby, BC) is mixed with deionized water. Two syringe pumps (Harvard Apparatus, MA) have been used for controlling oil/water flow rates in this experiment. A 3-way valve is used to connect the syringe pumps to the inlet port of ROC, for selective injection of oil/water phases. For collecting the volume of displaced oil, a precision volumetric glass cylinder (Corning Inc., NY) is connected to the outlet of ROC for measuring the displaced oil from the ROC during waterflooding.

Using the syringe pump, oil is introduced in the ROC at a constant injection rate of 50 μl min^{-1} and continued until the chip is completely filled with oil. Various 'dead volumes' in relation to the microfluidic connections and tubing are calculated. Dead volume was calculated by summing up the volumes in the inlet and outlet tubes, inlet and outlet ports, entrance and exit reasons and 3-way valve. Proper care has been taken while measuring the dead volume. Errors are estimated based on the least count of the instruments used for measurements. From the error analysis, it is found that the major source of error is from the precision volumetric glass cylinder. The total dead volume for the chip is calculated to be 816 μl ± 54 μl. The total quantity of resident oil in the ROC is calculated by subtracting the dead volumes from the total injected oil volume. In the next step, DI water containing the tracer dye is injected at a rate of 100 μl min^{-1} into the ROC. In this process, water displaces the resident oil from the ROC. The volume of displaced oil is measured in the collecting cylinder and compared to the original volume of resident oil present in the ROC. The choice of the flow rate is based on the current experimental constraints. In actual reservoir waterflooding case, a typical injection rate of 60 ml h^{-1} translates to an average pore velocity of 1 ft per day in typical oil fields. Such a high flow rate (1000 μl min^{-1}) can cause leakage and the flow transients will be too fast to be captured with the current optical set-up.

4. Results and discussion

The displacement of non-wetting fluid (oil) by wetting fluid (water) is investigated in the fabricated ROC. Wetting fluid (water) fills pores or throats with the highest threshold capillary pressure. The images of the waterflooding experiment have been taken at various places in the network and at different magnifications, in order to understand the average trend of fluid transport at these locations. Fig. 4 shows a series of images at one such specific network location taken before and during waterflooding. Fig. 4(a) shows the network completely filled with the oil phase (denoted by the green colour). Once waterflooding is initiated, oil slowly gets displaced due to the injection pressure and the water phase enters the network. Fig. 4(b) is the image at the same location of the network at a later instance of time (5 min from the start of waterflooding), with the oil/water interfaces visible due to the optical contrast between the oil and blue tracer dye. The green colour in the image represents the oil phase, while the blue colour represents water. Oil seems to be present in some pore-throats although the invading water phase had already passed these locations. Hence, water is not able to displace oil from each pore and throat uniformly, which mimics the natural waterflooding process one observes in the reservoir-scale.

The oil/water interfaces at the same network location but at a later instance of time (13 min from the start of waterflooding) is shown in Fig. 4(c). In this image, we notice the presence of similar characteristics of the oil/water phases as in the previous figure. The detailed displacement process captured in the video (see

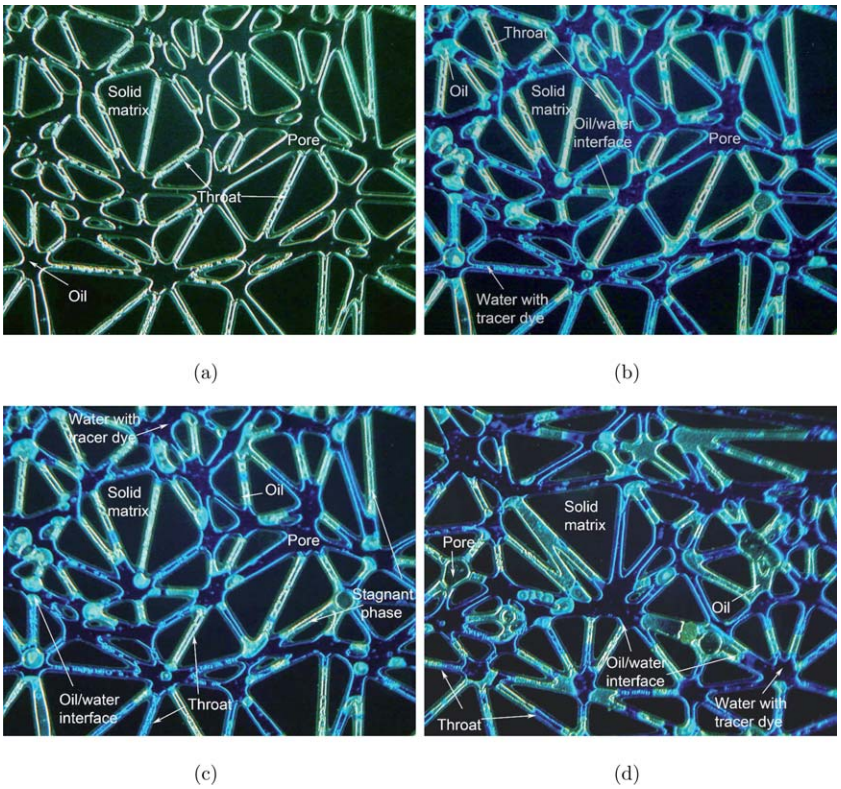

Fig. 4 Distribution of the oil phase (green colour) and water phase (blue colour) in the pore network during waterflooding experiments. (a) The presence of the oil phase at the start of the waterflooding process ($t = 0$); (b) Relative positions of the oil and water phases at $t = 5$ min; (c) Relative positions of the oil and water phases at $t = 13$ min. The presence of trapped oil is observed at the later part of the waterflooding process; (d) A different section of the pore network capturing the same dynamics of the oil and water phases at $t = 10$ min.

ESI†) shows that the velocity of oil displacement from throats has reduced with time. There are certain throats under observation, where the movement of the fluids is no longer occurring and stagnant phases of oil/water are noticed. Interested readers can refer to the video.† The stagnant phases imply that those pockets of resident oil phases will not be displaced by water flooding alone and they require other tertiary or enhanced recovery schemes, as observed in a practical oil reservoir. The first drop of water at the ROC outlet is observed at the time instance, which corresponds to Fig. 4(c). This process is often referred to as 'breakthrough' in reservoir engineering. From that time onward, both water and oil phases are found at the outlet of ROC. Fig. 4(d) represents the oil/water phases present at another location in the network during the experiment, at a time instance of 10 min from the start of waterflooding. Similar characteristics of displacement as those of the previous location can be observed, such as, stagnant phases in throats, *etc.*

It is observed that (from Fig. 4) the non-wetting phase (oil) was trapped primarily in the largest pore spaces, the pores with the highest aspect ratios (ratio of pore size to throat size), and the pores with the highest coordination numbers (number of throats connected to pores). Capillary forces are responsible for oil trapping. The capillary number (relative effect of viscous forces *versus* surface tension acting across an interface between oil and water) is very low (6×10^{-7}) based on the present experimental conditions. This low capillary number causes the discontinuous water phase flow in the network within 10 to 15 min of injection. The reduction in the capillary force results in reduced trapped oil in pore spaces.

Based on the volume data of total displaced oil, the fraction of recovered oil is calculated. A characteristic curve comparing the fraction of oil recovered with the injected water volume is presented in Fig. 5. This plot is similar to a recovery curve in traditional core-flooding experiments. In this case, original oil in place (OOIP) denotes the volume of oil inside the ROC, before waterflooding starts. We observe a linear pattern at the beginning of waterflooding (up to about 500 μl of water injection), implying that the invading water phase displaces the resident oil at the same rate as its injection. However, as more water is injected with time, the fraction of oil recovered is comparatively less, which has been explained in terms of the trapped volume of oil. The maximum fraction of oil recovered by this stimulated waterflooding process is about 65%, which corresponds to values obtained in typical core-flooding experiments.[2]

Proper care must be taken to extrapolate the results obtained from this ROC to the core-scale flooding and eventually to field-scale. Still, the ROC has numerous advantages over existing micromodels, since it uses the microstructural information of actual 3D reconstructed pore-spaces, which provides a better representation of the pore-structure of rock with pore connectivity. In addition, the ROC provides a better visualization of complex fluid flows and displacement mechanisms at the pore-scale.

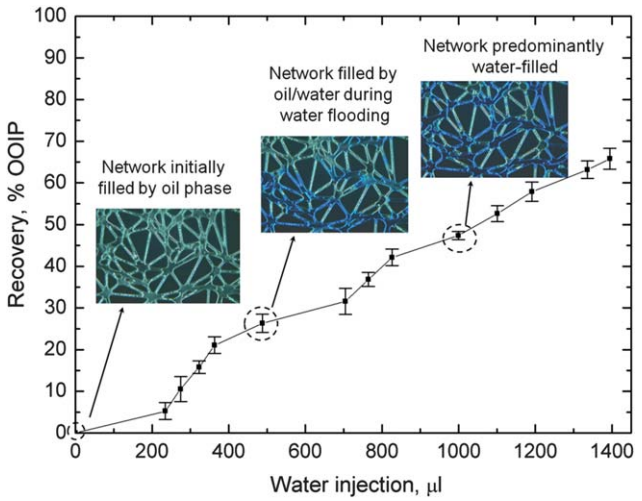

Fig. 5 Fraction of oil recovered in terms of original oil in place (OOIP) by injecting water at a constant flow rate of 100 μl min^{-1}, which is analogous to the recovery curve used in reservoir engineering by Hadia *et al.*[2] Insets show images of oil (green colour)/water (blue colour) phases corresponding to different time instances during the waterflooding process.

5. Conclusion

A novel concept for the miniaturization approach towards reservoir engineering and the study of waterflooding techniques on a chip related to oil recovery has been presented in this work. Instead of the usual approach of core-flooding or experimentation in micromodels containing random pore-network representing porous medium, a methodology has been described where reservoir-rock is converted to a microfluidic chip for the pore-scale study of oil displacement experiments. The sample core of such rock-specimens is characterized and reconstructed using advanced microscopy such as FIB-SEM, micro-CT, *etc.* Based on the reconstructed pore-space, a realistic pore network is designed and fabricated on silicon. Various parameters such as mean pore size and depth of the network have been designed in a manner such that this network is the most precise representation of an oil reservoir, and we coin the term 'Reservoir-on-a-Chip' (ROC) for this fabricated microfluidic device. Waterflooding experiments have been performed in this ROC. It is observed that, the invading water-phase cannot displace oil from all the pore-throats in the chip and oil remains as a stagnant phase at different locations due to capillary trapping. The analysis of the recovery curve based on the fraction of oil recovered reveals a similar type of oil-displacement pattern as obtained in a core-scale flooding experiment, which underlines the realization of the concept addressed in this study.

Acknowledgements

The authors gratefully acknowledge the financial support of Alberta Ingenuity (which is now part of Alberta Innovates) in the form of a scholarship for NSKG. The financial support from the Natural Sciences and Engineering Research Council is also acknowledged here.

References

1 G. Pope, *Society of Petroleum Engineers Journal*, 1996, **20**, 191–205.
2 N. Hadia, L. Chaudhari, S. K. Mitra, M. Vinjamur and R. Singh, *Exp. Therm. Fluid Sci.*, 2007, **32**, 355–361.
3 S. Bakke and P. E. Oren, *SPE Journal*, 1997, **2**, 136–149.
4 M. J. Blunt, *Curr. Opin. Colloid Interface Sci.*, 2001, **6**, 197–207.
5 M. J. Blunt, M. D. Jackson, M. Piri and P. H. Valvatne, *Adv. Water Resour.*, 2002, **25**, 1069–1089.
6 P. Valvatne and M. Blunt, *Water Resour. Res.*, 2004, **40**, W074061–W0740621.
7 I. Fatt, *Trans AIME*, 1956, **207**, 144–159.
8 A. A. Heiba, M. Sahimi, L. E. Scriven and H. T. Davis, *Society of Petroleum Engineers of AIME, (Paper) SPE*, 1982.
9 R. Lenormand, C. Zarcone and A. Sarr, *J. Fluid Mech.*, 1983, **135**, 337–353.
10 R. Lenormand, E. Touboul and C. Zarcone, *J. Fluid Mech.*, 1988, **189**, 165–187.
11 M. Blunt, *Curr. Opin. Colloid Interface Sci.*, 2001, **6**, 197–207.
12 R. I. Al-Raoush and C. S. Willson, *J. Contam. Hydrol.*, 2005, **77**, 67–89.
13 B. Bera, S. K. Mitra and D. Vick, *Micron*, 2011, **42**, 412–418.
14 C. S. Willson, R. W. Stacey, K. Ham and K. E. Thompson, *Proceedings of SPIE - The International Society for Optical Engineering*, 2004, 101–111.
15 J. D. Seymour and P. T. Callaghan, *AIChE J.*, 1997, **43**, 2096–2111.
16 W. E. Kenyon, *Nuclear Geophysics*, 1992, **6**, 153–171.
17 J. T. Geller and L. R. Myer, *J. Contam. Hydrol.*, 1995, **19**, 85–104.
18 G. Bohrer, H. Mourad, T. A. Laursen, D. Drewry, R. Avissar, D. Poggi, R. Oren and G. G. Katul, *Water Resour. Res.*, 2005, **41**, 1–17.
19 A. C. Gunde, B. Bera and S. K. Mitra, *Energy*, 2010, **35**, 5209–5216.
20 R. C. Acharya, S. E. A. T. M. V. der Zee and A. Leijnse, *Adv. Water Resour.*, 2007, **30**, 261–272.
21 Y. Zaretskiy, S. Geiger, K. Sorbie and M. Frster, *Adv. Water Resour.*, 2010, **33**, 1508–1516.
22 X. Zhan, L. M. Schwartz, M. N. Toksz, W. C. Smith and F. D. Morgan, *Geophysics*, 2010, **75**, F135–F142.
23 B. Manz, L. F. Gladden and P. B. Warren, *AIChE J.*, 1999, **45**, 1845–1854.
24 J. F. Chau, *Phys. Rev. E: Stat., Nonlinear, Soft Matter Phys.*, 2006, **74**, 056304.
25 R. D. Hazlett, S. Y. Chen and W. E. Soll, *J. Pet. Sci. Eng.*, 1998, **20**, 167–175.
26 T. Ramstad, P. E. Oren and S. Bakke, *SPE Journal*, 2010, **15**, 923–933.
27 T. Ramstad, P. E. Oren and S. Bakke, *Proceedings - SPE Annual Technical Conference and Exhibition*, 2009, 2561–2576.
28 A. S. Al-Kharusi and M. J. Blunt, *J. Pet. Sci. Eng.*, 2007, **56**, 219–231.
29 H. Dong and M. J. Blunt, *Phys. Rev. E: Stat., Nonlinear, Soft Matter Phys.*, 2009, **80**, 036307.
30 N. A. Idowu and M. J. Blunt, *International Petroleum Technology Conference, IPTC 2008*, 2008, 1183–1198.
31 N. A. Idowu and M. J. Blunt, *Transp. Porous Media*, 2010, **83**, 151–169.
32 S. Litster, D. Sinton and N. Djilali, *J. Power Sources*, 2006, **154**, 95–105.
33 P. E. Oren and W. V. Pinczewski, *Transp. Porous Media*, 1995, **20**, 105–133.
34 M. I. J. Van-Dijke, K. Sorbie, M. Sohrabi and A. Danesh, *J. Pet. Sci. Eng.*, 2006, **52**, 71–86.
35 M. I. J. Van-Dijke, K. S. Sorbie, M. Sohrabi and A. Danesh, *SPE Journal*, 2004, **9**, 57–66.
36 M. Sohrabi, A. Danesh and M. Jamiolahmady, *Transp. Porous Media*, 2008, **74**, 239–257.
37 D. Broseta, F. Medjahed, J. Lecourtier and M. Robin, *SPE Advanced Technology Series*, 1995, **3**, 103–112.
38 D. Broseta and F. Medjahed, *J. Colloid Interface Sci.*, 1995, **170**, 457–465.
39 H. E. Meybodi, R. Kharrat and X. Wang, *Transp. Porous Media*, 2011, **89**, 97–120.
40 B. Y. Jamaloei and R. Kharrat, *Transp. Porous Media*, 2009, **76**, 199–218.
41 B. Y. Jamaloei and R. Kharrat, *Transp. Porous Media*, 2010, **81**, 1–19.

42 B. Y. Jamaloei, K. Asghari, R. Kharrat and F. Ahmadloo, *J. Pet. Sci. Eng.*, 2010, **72**, 251–269.
43 C. L. Perrin, K. S. Sorbie, P. M. J. Tardy and J. P. Crawshaw, *67th European Association of Geoscientists and Engineers, EAGE Conference and Exhibition, incorporating SPE EUROPE2005-Extended Abstracts*, 2005, 933–940.
44 S. A. Bowden, J. M. Cooper, F. Greub, D. Tambo and A. Hurst, *Lab Chip*, 2010, **10**, 819–823.
45 S. A. Bowden, R. Wilson, J. Parnell and J. M. Cooper, *Lab Chip*, 2009, **9**, 828–832.
46 D. Sen, D. Nobes and S. K. Mitra, *Microfluid. Nanofluid.*, 2011, DOI: 10.1007/s10404-011-0862-x.
47 V. Berejnov, N. Djilali and D. Sinton, *Lab Chip*, 2008, **8**, 689–693.
48 F. Aktas, T. Clemens, L. M. Castanier and A. R. Kovscek, *Proceedings - SPE Symposium on Improved Oil Recovery*, 2008, 384–394.
49 M. Buchgraber, T. Clemens, L. M. Castanier and A. R. Kovscek, *SPE Reservoir Eval. Eng.*, 2011, **14**, 269–280.
50 M. Buchgraber, T. Clemens, L. M. Castanier and A. R. Kovscek, *Proceedings - SPE Annual Technical Conference and Exhibition*, 2009, 78–96.
51 R. Hazlett, *Transp. Porous Media*, 1995, **20**, 21–35.
52 R. wirth, *Chem. Geol.*, 2009, **261**, 217–229.
53 J. Wilson, W. Kobsiriphat, R. Mendoza, H. Chen, J. Hiller, D. Miller, K. Thornton, P. Voorhees, S. Adler and S. Barnett, *Nat. Mater.*, 2006, **5**, 541–544.
54 N. S. K. Gunda, H. Choi, A. Berson, B. Kenney, K. Karan, J. Pharoah and S. K. Mitra, *J. Power Sources*, 2011, **196**, 3592–3603.
55 M. Sahimi, A. A. Heiba, H. T. Davis and L. E. Scriven, *Chem. Eng. Sci.*, 1986, **41**, 2123–2136.
56 N. Karadimitriou, S. Hassanizadeh and P. Kleingeld, *First International Conference on Frontiers in Shallow Subsurface Technology*, 2010.
57 K. J. Seu, A. P. Pandey, F. Haque, E. A. Proctor, A. E. Ribbe and J. S. Hovis, *Biophys. J.*, 2007, **92**, 2445–2450.

